New Phytologist

Research

Heatwave breaks down the linearity between sun-induced fluorescence and gross primary production

David Martini[1], Karolina Sakowska[2], Georg Wohlfahrt[3], Javier Pacheco-Labrador[1], Christiaan van der Tol[4], Albert Porcar-Castell[5], Troy S. Magney[6], Arnaud Carrara[7], Roberto Colombo[8], Tarek S. El-Madany[1], Rosario Gonzalez-Cascon[9], María Pilar Martín[10], Tommaso Julitta[11], Gerardo Moreno[12], Uwe Rascher[13], Markus Reichstein[1], Micol Rossini[8] and Mirco Migliavacca[1,14]

[1]Max Planck Institute for Biogeochemistry, 07745 Jena, Germany; [2]Institute of BioEconomy, National Research Council (IBE-CNR), 38010 San Michele all'Adige (TN), Italy; [3]Department of Ecology, University of Innsbruck, Sternwartestrasse 15, 6020 Innsbruck, Austria; [4]Faculty of Geo-Information Science and Earth Observation (ITC), University of Twente, 7500 AE Enschede, the Netherlands; [5]Optics of Photosynthesis Laboratory, Institute for Atmospheric and Earth System Research (INAR/Forest Sciences) and Viikki Plant Science Center, University of Helsinki, Finland; [6]Department of Plant Sciences, University of California, Davis, CA 95616, USA; [7]Centro De Estudios Ambientales Del Mediterráneo, 46980 Valencia, Spain; [8]Earth and Environmental Sciences Department, University of Milano-Bicocca, Milan, Italy; [9]Department of Environment, National Institute for Agriculture and Food Research and Technology (INIA), 28040 Madrid, Spain; [10]Environmental Remote Sensing and Spectroscopy Laboratory (SpecLab), Spanish National Research Council (CSIC), 28037 Madrid, Spain; [11]JB Hyperspectral Devices, 40225 Düsseldorf, Germany; [12]Universidad de Extremadura, 10600 Plasencia, Spain; [13]Institute of Bio- and Geosciences, IBG-2: Plant Sciences, Forschungszentrum Jülich, Jülich, Germany; [14]European Commission, Joint Research Centre, Ispra (VA) 21027, Italy

Authors for correspondence:
David Martini
Email: *dmartini@bgc-jena.mpg.de*

Mirco Migliavacca
Email: *mirco.migliavacca@ec.europa.eu*

Received: *16 May 2021*
Accepted: *21 November 2021*

New Phytologist (2022) **233:** 2415–2428
doi: 10.1111/nph.17920

Key words: extreme events, gross primary production (GPP), heatwave, nonphotochemical quenching, photosynthesis, sun-induced fluorescence.

Summary

- Sun-induced fluorescence in the far-red region (SIF) is increasingly used as a remote and proximal-sensing tool capable of tracking vegetation gross primary production (GPP). However, the use of SIF to probe changes in GPP is challenged during extreme climatic events, such as heatwaves.
- Here, we examined how the 2018 European heatwave (HW) affected the GPP–SIF relationship in evergreen broadleaved trees with a relatively invariant canopy structure. To do so, we combined canopy-scale SIF measurements, GPP estimated from an eddy covariance tower, and active pulse amplitude modulation fluorescence.
- The HW caused an inversion of the photosynthesis–fluorescence relationship at both the canopy and leaf scales. The highly nonlinear relationship was strongly shaped by nonphotochemical quenching (NPQ), that is, a dissipation mechanism to protect from the adverse effects of high light intensity. During the extreme heat stress, plants experienced a saturation of NPQ, causing a change in the allocation of energy dissipation pathways towards SIF.
- Our results show the complex modulation of the NPQ–SIF–GPP relationship at an extreme level of heat stress, which is not completely represented in state-of-the-art coupled radiative transfer and photosynthesis models.

Introduction

Gross primary production (GPP) of terrestrial ecosystems represents the most important flux in the global carbon cycle (Beer *et al.*, 2010), which provides ecosystem services of critical importance for society (Holmberg *et al.*, 2019). Anthropogenic climate change has increased global temperatures and the frequency and intensity of climate extremes such as heatwaves and droughts (Bindoff *et al.*, 2014), which have had a considerable effect on GPP (Reichstein *et al.*, 2013). Gross primary production can be estimated by means of proximal and remote sensing (RS), particularly through the use of sun-induced fluorescence in the far-red region (SIF) (Damm *et al.*, 2010; Pacheco-Labrador *et al.*, 2019a). Top-of-the-canopy SIF measurements contain information on the radiation emitted by plant chlorophyll when plants are exposed to solar radiation, mediated by canopy architecture through reabsorption and multiple scattering escape probability of fluorescence (Fesc) (Yang & van der Tol, 2018). Sun-induced fluorescence in the far-red region region is used to predict GPP as it is related to both the amount of absorbed photosynthetic active radiation (APAR) and the efficiency with which APAR is used to drive photosynthesis light-use efficiency of photosynthesis (LUE_p) (Zhang *et al.*, 2014). Therefore, SIF has the potential to quantify the effect of extreme events such as heatwaves on photosynthetic activity (Ač *et al.*, 2015). Nevertheless, there is a need to explore the mostly unknown mechanistic relationship between SIF and GPP during rapid extreme heat stress (Wohlfahrt *et al.*, 2018; Magney *et al.*, 2019).

Both the light-dependent reactions of photosynthesis and SIF originate at the photosystem level. When a chlorophyll molecule is excited by a photon of light, the available energy can be allocated to photochemistry, emitted as fluorescence (that contributes to the top-of-the-canopy SIF signal), or dissipated as heat through nonphotochemical quenching (NPQ) (Kitajima & Butler, 1975), a process involving xanthophyll cycle de-epoxidation. Because photochemistry and NPQ are physiologically modulated (Porcar-Castell *et al.*, 2014) and respond to different environmental conditions, it is complicated to find a universal linear relationship between photochemistry and SIF, without information about NPQ, especially under stress conditions.

An understanding of the trade-offs between these processes can be achieved by combining canopy-scale passive (i.e. SIF) with leaf-level active pulse amplitude modulation (PAM) fluorescence techniques; the latter of which can be used to derive parameters such as yields of photochemistry (ϕP) (Genty *et al.*, 1989) and fluorescence (ϕF) (Atherton *et al.*, 2019), and NPQ (Cailly, 1996). Active fluorescence data at high temporal resolution (e.g. hourly) suggest that the relationship between ϕF and ϕP at the leaf level is highly nonlinear and strongly dependent on illumination conditions and NPQ (Porcar-Castell *et al.*, 2014). Under typical high-radiation conditions, ϕP decreases in response to NPQ increase, driving the positive SIF–photochemistry relationship ('NPQ phase') (Porcar-Castell *et al.*, 2014). van der Tol *et al.* (2014) reported that at high light and stress conditions, various crops showed a negative ϕF–ϕP relationship (the 'NPQ-saturation phase'). However, to our knowledge, there have been no observations of the 'NPQ-saturation phase' for plants experiencing heat stress, and it is unclear how this mechanism emerges at the canopy scale as suggested by Magney *et al.* (2020). Nonphotochemical quenching is crucial to understand and model the GPP–SIF relationship. Although the photochemical reflectance index (PRI) can be used track NPQ, its use is challenging at the canopy scale because canopy structure can be a confounding factor (Wong & Gamon, 2015). The integration of leaf and canopy-scale fluorescence has the potential to explain the scale dependence of trade-offs between NPQ, photochemistry and fluorescence (Magney *et al.*, 2017), and therefore can help to better understand the physiological information contained in SIF.

Extreme events such as heatwaves can represent natural experiments, in which increases in NPQ (Georgieva & Yordanov, 1994) can alter GPP–SIF dynamics. Generally, deciduous trees, crops, and grasslands react to heatwaves through a combination of physiological (e.g. increase in NPQ and/or transpiration (Drake *et al.*, 2018)) and structural changes (reduction in leaf area index (LAI), chlorophyll degradation). Evergreen trees, particularly in the Mediterranean and semiarid regions, can withstand extreme temperatures of short duration without showing significant pigment degradation or changes in canopy structure (Teskey *et al.*, 2015), primarily relying on physiological adaptation for coping with extreme temperatures (Garcia-Plazaola *et al.*, 2008). Evergreen broadleaved trees therefore represent an excellent test case to study the effect of extreme heatwaves on the GPP–SIF relationship independently of the variations in chlorophyll content and APAR. Here, we make use of data from the 2018 European heatwave (HW) that resulted in record-breaking temperatures (Bastos *et al.*, 2020) in Western Europe (Barriopedro *et al.*, 2020). During the first week of August, the western side of the Iberian Peninsula experienced daily temperature anomalies compared with long-term observations up to 9°C, caused by a Saharan air intrusion, leading to the most extreme event ever recorded in the region (Sousa *et al.*, 2019; Barriopedro *et al.*, 2020).

This study aims to shed light on the relationship between GPP and SIF during an extreme HW when changes in canopy structure are minimal. Our goals are two-fold: First, we wish to understand the effect of the HW on the GPP–SIF relationship. In particular, we want to investigate what role NPQ plays in shaping the GPP–SIF relationship at high heat-stress levels. Second, we investigated if a state-of-the-art radiative transfer and photosynthesis model can reproduce NPQ, which is critical to obtain SIF, at high heat stress. To do so, we used data from Mediterranean evergreen oak trees (*Quercus ilex*) at the study site Majadas de Tiétar (ES-LMa), where we measured canopy-scale SIF, GPP estimated with the eddy covariance technique and active PAM fluorescence.

Materials and Methods

Study site

The study was conducted in a Mediterranean open woodland, a typical Iberian *dehesa* in western Spain (39°56′24.68″N, 5°45′50.27″W; Majadas de Tiétar, Cáceres, Extremadura, FLUXNET site ES-LMa) (Supporting Information Fig. S1). The ecosystem is composed of an herbaceous layer and scattered evergreen broadleaved trees, mainly *Quercus ilex* L. subsp. *ballota* [Desf.] Samp. (Holm oak). Trees fractional cover was *c.* 20%, while the average horizontal and vertical crown radius was 4.2 m (σ = 0.9 m) and 2.7 m (σ = 0.9 m), respectively (Pacheco-Labrador *et al.*, 2019b).

The climate is Mediterranean, characterised by a hot and dry summer. The annual precipitation value is *c.* 650 mm (falling mostly from autumn to spring). The mean annual temperature is 16°C. The study was conducted from June 2018 to August 2018, when the herbaceous layer was senesced (Luo *et al.*, 2018, 2020), and the trees were the only active vegetation (El-Madany *et al.*, 2020). From 2 August to 6 August 2018, the ecosystem experienced a heatwave (Barriopedro *et al.*, 2020) with a 5-d average of daily maximum air temperature (T_{air}) of 43.2°C and daily maximum vapour pressure deficit (VPD) of 76.1 hPa (Fig. S2). Extensive site details are available in earlier publications (El-Madany *et al.*, 2018). The days considered part of the heatwave are the 5 d from the 2 August 2018 to 6 August 2018, according to Sousa *et al.* (2019); while the days considered pre-heatwave are the 25 July 2018 to 1 August 2018.

Sun-induced fluorescence observations

The spectral measurements were collected using the FloX (JB Hyperspectral Devices, Düsseldorf, Germany), a field spectrometer

designed for continuous high-resolution spectral measurements for SIF retrieval with technical specifications in terms of spectral coverage, resolution and signal-to-noise ratio (SNR) coherent with the FLEX mission instrument specifications (Julitta *et al.*, 2017). The FloX was equipped with two spectrometers: (1) QEPro (Ocean Optics, Largo, FL, USA) with high spectral resolution (full width at half maximum *c.* 0.3 nm) in the fluorescence emission range 650–800 nm; (2) FLAME S (Ocean Optics) covering the full range of visible–near-infrared (full width at half maximum *c.* 1.7 nm). The spectrometer entrance slit was split into two optical fibres leading to a cosine receptor measuring the downwelling radiance and a bare fibre measuring the canopy upwelling radiance. The spectrometers were housed in a thermally regulated box, keeping the internal temperature constant at 20°C to avoid dark current drift and spectral shifts related to temperature changes. The thermoelectric cooler of the QEPro was set to 20°C to control the back thinned CCD detector SNR (nominal SNR > 1000 : 1). The integration time of the spectrometers was optimised for each channel (down-looking and up-looking channels) at the beginning of each automatic measurement cycle. Two dark spectra were systematically recorded at each measurement cycle.

The FloX system was installed on a 10 m tall optical observation tower located near the eddy covariance (EC) tower. An upward facing fibre cable equipped with a cosine diffuser measured the downwelling irradiance, the upwelling radiance was measured with a bare fibre (25° field of view) pointing roughly north at a Holm oak crown at *c.* 2 m distance from the tower and slightly off-nadir (*c.* 10°). From the measured spectra we retrieved sun-induced fluorescence in the red (O_2-B band, 687 nm) and far-red (O_2-A band, 760 nm) regions, referred to as SIF_B and SIF respectively, using both the improved Fraunhofer line depth (iFLD) and the spectral fitting method (SFM) (Meroni *et al.*, 2009). Sun-induced fluorescence in the far-red region and SIF_B retrieved with iFLD and SFM were extremely similar (Table S1). Therefore, in the article we present only the iFLD, as it is less sensitive to noise compared with other retrieval methods (Cendrero-Mateo *et al.*, 2019). The integrated SIF ($SIF_{660–840}$) was calculated as: $SIF_{660–840} = 39.2435 \times SIF_B + 83.6814 \times SIF$ following Moreno *et al.* (2015). We applied a filter to remove measurements that were taken at high solar zenith angles (SZA < 50), which results in retrieval errors and nonlinear response of the cosine optics (Julitta *et al.*, 2016). We computed a series of additional vegetation indices: the normalised difference vegetation index (NDVI), the near-infrared reflectance of vegetation index (NIR_V) (Badgley *et al.*, 2017) and the PRI (Gamon *et al.*, 1997), derived from reflectance at 531 and 570 nm. Spectral measurements were taken at an interval of *c.* 2 min, and then averaged over 1-h periods.

To reduce the effect of canopy structure on the fluorescence signal and to derive a more physiological proxy of fluorescence we calculated the escape probability of SIF (Fesc) following Zeng *et al.* (2019) (Eqn 1). We used the method proposed by Zeng *et al.* (2019) as the assumption of high LAI and low contribution of soil to the reflectance were met given the experimental design:

$$\text{Fesc} = \frac{\text{NIR}_V}{f_{\text{APAR}}} \quad \text{Eqn 1}$$

Fraction of absorbed photosynthetically active radiation (f_{APAR}) and APAR were estimated from incoming and reflected radiance following Damm *et al.* (2010) and (Li & Moreau, 1996; Moreau & Li, 1996) (Eqn 2):

$$\text{APAR} = (\text{PAR}_{\text{inc}} - \text{PAR}_{\text{refl}}) \times \text{RAPAR} \quad \text{Eqn 2}$$

(PAR_{inc}, the incoming photosynthetic active radiation (PAR); PAR_{refl}, the reflected PAR; RAPAR, the ratio of PAR absorbed by the green canopy to the PAR absorbed by all surface materials) and it was calculated as shown in Eqn 3:

$$\text{RAPAR} = 0.105 - 0.323 \times \text{NDVI} + 1.468 \times \text{NDVI}^2 \quad \text{Eqn 3}$$

Total SIF (SIF_{tot}) was calculated as in Eqn 4:

$$\text{SIF}_{\text{tot}} = \frac{\text{SIF}}{\text{Fesc}} \quad \text{Eqn 4}$$

The light-use efficiency of photosynthesis (LUE_p) was calculated as in Eqn 5:

$$\text{LUE}_p = \frac{\text{GPP}}{\text{APAR}} \quad \text{Eqn 5}$$

Light-use efficiency of fluorescence emission, LUE_f was calculated as in Eqn 6:

$$\text{LUE}_f = \frac{\text{SIF}}{(\text{APAR} \times \text{Fesc})} \quad \text{Eqn 6}$$

APAR was estimated in mW m^{-2} nm^{-1} sr^{-1} and then converted to μmol m^{-2} s^{-1} for the LUE_p calculation in Fig. 3(b). All data were presented at an hourly scale, except for Figs 1, 2(a–d), S3 for which midday means (between 11 and 13 coordinated universal time (UTC)) were used.

Leaf-level active chlorophyll fluorescence and chlorophyll content

Diurnal variation in active chlorophyll fluorescence was measured with a MONI-PAM Multi-Channel Chlorophyll Fluorimeter (Walz, Effeltrich, Germany) composed of a data acquisition unit and five emitter–detector units (heads). The system was equipped with solar panels as a power supply and operated in stand-alone mode. The five heads of the MONI-PAM were installed on south-facing branches of a *Quercus ilex* tree located within the EC footprint near the tree on which FloX measurements were performed (Fig. S1e). Branches were accessed using a permanent scaffold, and measurements were performed on leaves flushed in 2018. Active fluorescence signals included instantaneous fluorescence and maximal fluorescence along with incident PAR and T_{air}, and were recorded at 10-min and 1-h frequencies, during the daytime and night-time,

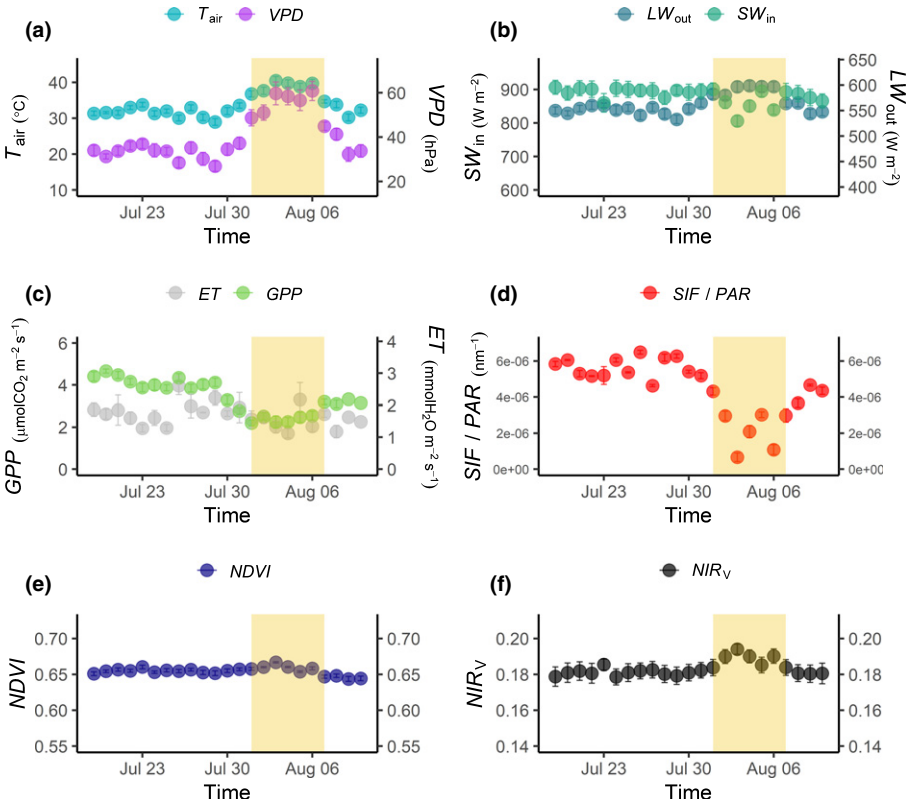

Fig. 1 Daily means of (a) air temperature (T_{air}), vapour pressure deficit (VPD), (b) shortwave incoming radiation (SW_{in}), longwave outgoing radiation (LW_{out}), (c) gross primary production (GPP) and evapotranspiration (ET), (d) sun-induced fluorescence at 760 nm (SIF) divided by photosynthetic active radiation (PAR) (SIF/PAR), (e) normalised difference vegetation index (NDVI), (f) near-infrared reflectance of vegetation (NIR_V). Daily values in (a–f) are computed between 11 and 13 Coordinated Universal Time (UTC). The yellow rectangle represents the heatwave (HW) period.

respectively. For active fluorescence data, the hours from 11 to 16 UTC were considered, as the leaves measured by the MONI-PAM were shaded before 11 UTC, as shown by the high ϕP and low NPQ values between 8 and 10 UTC (Fig. S4d,f). MONI-PAM data were used to derive NPQ, the yield of NPQ (ϕNPQ), the reversible component of NPQ (NPQ_r), the sustained component of NPQ (NPQ_s) and the yield of photochemistry (ϕP) according to Porcar-Castell (2011). The maximum value at night of quantum yield of photosystem II (ΦP_{max}), corresponding to the widely used F_v/F_m, was calculated according to Porcar-Castell (2011). For the calculation of NPQ, a reference maximum fluorescence (F_{mR}) value was obtained during a period in which at night-time the ΦP_{max} was 0.81, which is within the range of nonstressed ΦP_{max} in Holm oak (Ogaya & Peñuelas, 2003). The yield of fluorescence (ϕF) was calculated as detailed in Porcar-Castell *et al.* (2014). Relative light saturation of photosynthesis (x) is a scaling factor that describes the degree of photochemical impairment and was calculated following van der Tol *et al.* (2014). Details regarding the calculation of the MONI-PAM parameters can be found in the following R package developed by our group (https://github.com/davidmartini90/pam). For the estimation of the parameters with the PAM, we used the prevailing assumption of perfect connectivity between PSII units (lake model assumption), for which is still unclear whether is valid under stress (Porcar-Castell, 2011). The above parameters were obtained for each MONI-head and averaged across all heads.

A soil plant analysis development (SPAD) chlorophyll meter was used to estimate leaf chlorophyll status. Soil plant analysis development measures transmittance of red (650 nm) and infrared (940 nm) radiation through the leaf (Uddling *et al.*, 2007). The SPAD measurements provide an indicator of chlorophyll content in relative units (SPAD values). Soil plant analysis development values measured in *Quercus ilex* at the same experimental site in previous studies were found to be linearly related ($R^2 = 0.91$) with chlorophyll $a + b$ obtained in the laboratory (Gonzalez-Cascon *et al.*, 2017). Soil plant analysis development measurements took place on 20 July 2018 (before the HW) and 4 August 2018 (during the HW), and were carried out on the tree measured with the FloX and the tree measured with the MONI-PAM. In each tree, two branches were measured (12 leaves per branch), dividing between current year leaves (new leaves) and previous year leaves (old leaves).

Biometeorological parameters and carbon fluxes

Biometeorological variables and surface gas exchange have been measured at the site since 2014 and we used data from June 2018 to July 2018. During this period the herbaceous layer was completely dry. Therefore, the fluxes measured were representative of only the tree functioning as shown previously (Perez-Priego *et al.*, 2017; Perez-Priego *et al.*, 2018; El-Madany *et al.*, 2020) in which EC-derived water fluxes were compared with independent water fluxes of the herbaceous layer obtained with the lysimeters and sap flow measurements of the trees. An EC system consisting of a three-dimensional sonic anemometer (R3-50; Gill LTD, Lymington, UK) and an infrared gas analyser (LI-7200; Li-Cor Bioscience, Lincoln, NE, USA) was used to measure dry mixing ratios of CO_2 and H_2O at a height of 15.5 m aboveground. Shortwave incoming radiation (SW_{in}) and

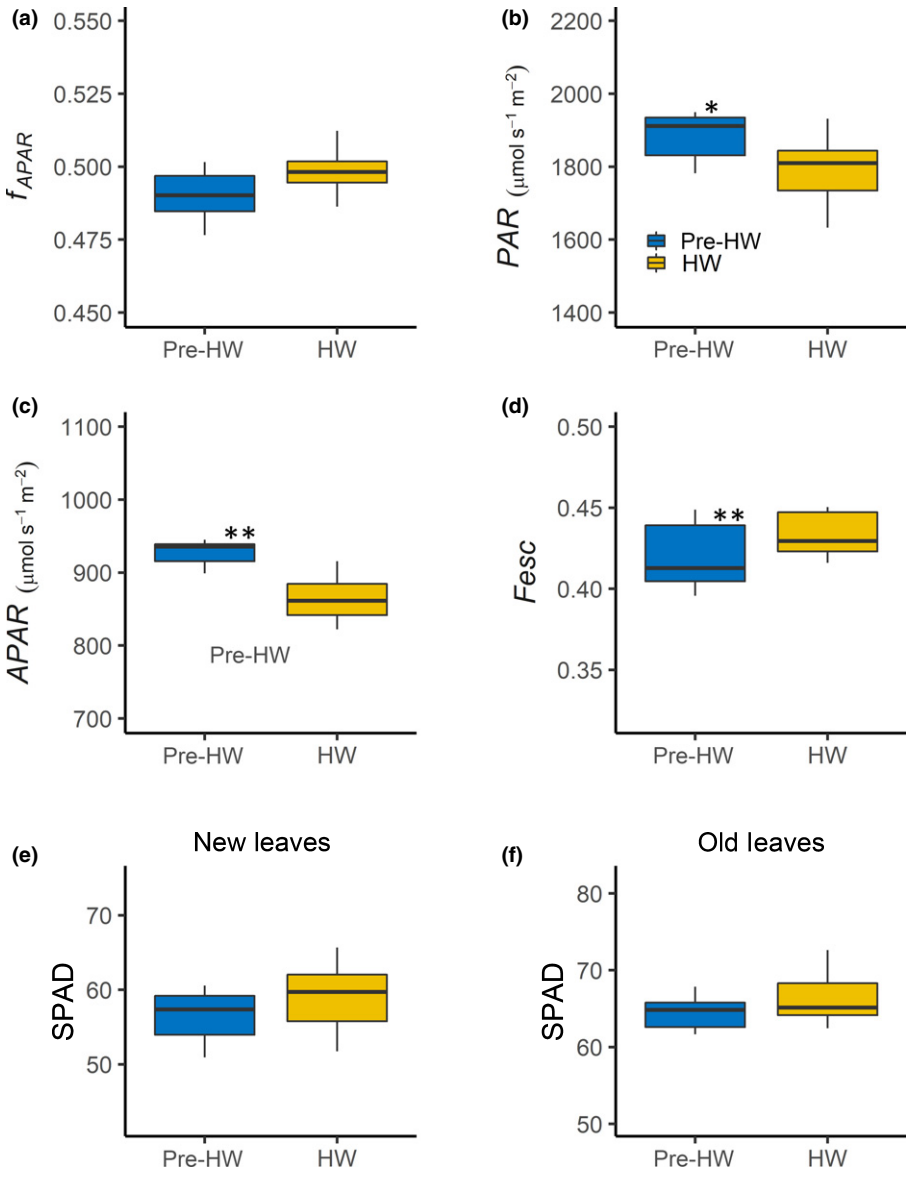

Fig. 2 Boxplot of (a) fraction of absorbed photosynthetic active radiation (f_{APAR}); (b) photosynthetic active radiation (PAR); (c) absorbed photosynthetic active radiation (APAR); (d) escape probability of SIF (Fesc); and (e, f) values from soil plant analysis development (SPAD) chlorophyll meter for old leaves (i.e. leaves flushed in previous years) and new leaves (i.e. leaves flushed in the 2018), respectively. The boxes for the pre-heatwave (pre-HW) period values are blue while for the heatwave (HW) period in yellow. Daily values of f_{APAR}, PAR, APAR and Fesc are computed between 11 and 13 Coordinated Universal Time (UTC). **, $P < 0.01$; *, $P < 0.05$ according to analysis of variance (ANOVA) test. No significant differences are observed in (a, e, f). In the boxplot the thick lines represent the median and the lower and upper hinges correspond to the 25th and 75th percentiles. The upper/lower whiskers extend from the hinge to the largest/smallest value no further than 1.5× interquantile range.

longwave outgoing radiation (LW_{out}) were measured with a ventilated net radiometer (CNR4; Kipp and Zonen, Delft, the Netherlands). Air temperature (T_{air}) and relative humidity (rH) were measured with a combined Pt-100 temperature and capacitive humidity sensor (CPK1-5; MELA Sensortechnik, Bondorf, Germany). Fluxes were computed using EddyPro v.6.2.0 (Fratini & Mauder, 2014) as described in El-Madany *et al.* (2018). Quality check of the fluxes was carried out according to Mauder & Foken (2011). The storage flux was computed using a vertical profile of CO_2 according to Falge *et al.* (2001). The u*-threshold (*c.* 0.13 m s^{-1}) was estimated according to Papale *et al.* (2006). The measured net ecosystem exchange (NEE) was partitioned into GPP using both night-time partitioning (Reichstein *et al.*, 2005) and daytime partitioning (Lasslop *et al.*, 2010) methods as implemented in the REddyProc 0.7–1 R package (Papale *et al.*, 2006; Wutzler *et al.*, 2018). For the analysis we retained only data coming from measured NEE and latent heat data, or gap-filled data with high confidence (i.e. quality flag 0 and 1 (Wutzler *et al.*, 2018)). In the main text only the GPP from the daytime partitioning technique is reported. We decided to use the GPP from the daytime partitioning because the GPP derived from night-time partitioning was noisier (e.g. (Lasslop *et al.*, 2010)), particularly when measured NEE was relatively low, as during the heat wave. GPP–SIF and the GPP–VPD relationships were consistent independently to the CO_2 flux partitioning method (Tables S2, S3), as well as the method used for retrieval of SIF (Tables S1, S3).

The EC and biometeorological data were averaged at hourly temporal resolution to smooth the effect of the random error on the measurements (Damm *et al.*, 2010). Evapotranspiration (ET) was obtained from latent heat flux measurements, the surface conductance (gs) was obtained by inverting the Penman–Monteith equation (Beven, 1979). Aerodynamic resistance was calculated following Thom (1972) and removed before the calculation of gs. Calculations were conducted using the bigleaf R package (Knauer *et al.*, 2018).

Statistical analysis

Significant differences between groups (HV and pre-HW) were calculated using analysis of variance (ANOVA) (Girden, 1992). To test differences in the slope of the NPQ–VPD relationship between the pre-HW period and the HW period, an analysis of covariance (ANCOVA) was used (Rutherford, 2001). Regressions were performed with linear ordinary least squares and second-degree polynomial regression. Selection of the regression method was based on lowest Akaike information criterion. Correlations coefficients were calculated using Spearman's rank correlation (R).

Results

Effect of the heatwave on SIF, NDVI and NIR_V

During the HW we observed an increase of 7.2°C and 22 hPa in daily mean T_{air} and VPD, respectively (Fig. 1a), compared with the pre-HW period (i.e. 7 d before the heatwave). The 5-d average of daily maximum T_{air} and VPD of 43.2°C and 76.1 hPa, respectively, represented a substantial positive anomaly compared with that measured at the site since 2004 (Fig. S2). As the HW was caused by a Saharan air intrusion (Sousa *et al.*, 2019), which was accompanied by higher than average dust levels, we observed a 4.9% mean decrease in SW_{in} ($P < 0.01$), and therefore also PAR. After the HW the SW_{in} returned to the initial values. As a consequence of heat stress, LW_{out} increased by 7.2% ($P < 0.01$) (Fig. 1b). The trees responded to the HW by decreasing photosynthesis (32.2% mean decrease of midday – between 11 and 13 UTC – GPP, $P < 0.01$) (Fig. 1c) and by sharply diminishing midday SIF (Fig. 1d). Sun-induced fluorescence in the far-red region normalised by PAR exhibited a massive decline, with a mean decrease of 64.1% ($P < 0.01$) with respect to the pre-HW level (Fig. 1d). Evapotranspiration did not significantly vary between the pre-HW and HW periods (Fig. 1c) ($P = 0.129$), but a gradual decline was observed during the HW. Fig. S5 shows a strong sensitivity of gs to VPD, with lower gs during the HW. The strong physiological response of the vegetation contrasted with the relative stability of two spectral indices, the NDVI and the NIR_V (Fig. 1e,f), which can be considered indicators of vegetation canopy greenness. Both indices increased significantly ($P = 0.02$, $P < 0.01$ for NDVI and NIR_V, respectively) with the HW, although their increment was modest: 0.7% and 4.7% for NDVI and NIR_V, respectively. Simulations with the soil canopy observation, photochemistry and energy fluxes (SCOPE), a state-of-the-art radiative transfer–photosynthesis coupled model, showed that this increase can be explained by increased diffuse radiation during the HW (Fig. S6).

f_{APAR} and chlorophyll remain unaltered

The HW did not cause statistically significant changes in f_{APAR} ($P = 0.07$) (Fig. 2a), which remained stable *c.* 0.49. Similarly, chlorophyll concentration estimated with SPAD (as described in the Materials and Methods section) did not show significant differences for both the leaves flushed in 2018 ($P = 0.06$) (Fig. 2e) and in the previous year ($P = 0.052$) (Fig. 2f). Absorbed photosynthetic active radiation decreased (6.9% mean decrease) during the HW due to the reduction in PAR (5% mean decrease) (Fig. 2a,b). Escape probability of fluorescence instead showed a modest, yet significant ($P < 0.01$), increase (from a mean value of 0.418 ± 0.011 during the pre-HW to 0.432 ± 0.009 during the HW) (Fig. 2d). Due to the small change in Fesc, we could not definitively rule out a change in canopy structure during the HW. Still, it was clear from the negligible changes in vegetation indices and f_{APAR} that the response of *Quercus ilex* to extreme heat was primarily physiological and only marginally structural.

Nonlinear GPP–SIF relationship at hourly time scale during the heatwave

Our study revealed a nonlinear relationship between GPP and SIF, when considering both the pre-HW and HW periods. During the pre-HW period GPP and total SIF_{tot} exhibited a positive relationship ($R = 0.52$, $P < 0.01$), while during the HW their relationship was negative ($R = -0.36$, $P = 0.034$) (Fig. 3a). This pattern was even more pronounced when the efficiencies of both processes were considered, as shown by the relationship between LUE_p and LUE_f (Figs 3b, S7).

A similar pattern was observed at the leaf level, as the relationship between ϕP and ϕF was negative during the HW ($R = -0.61$, $P < 0.01$) and positive during the pre-HW period ($R = 0.64$, $P < 0.01$). During the pre-HW period the ϕP−ϕF relationship showed a clear hysteresis (Fig. S8) as for the same ϕF, ϕP showed lower values in the morning and higher values in the afternoon.

The relationship between GPP and indices such as NDVI, PRI, and NIR_V (Fig. S9) differed strongly from the one exhibited by GPP and SIF. Photochemical reflectance index showed a strong linear relationship ($R = 0.86$, $P < 0.01$) with GPP (Fig. S9a), which indicated the important role of NPQ dissipation during the HW. Moreover, NPQ and PRI were strongly correlated (Fig. S10d), suggesting that, given the negligible changes in canopy structure, PRI was a good indicator of NPQ processes despite the different scales at which they were measured (leaf and canopy). Normalised difference vegetation index showed no significant relationship with GPP (Fig. S9b), while NIR_V showed a negative relationship ($R = -0.69$, $P < 0.01$) (Fig. S9c). The negative relationship could be explained by GPP reaching its maximum in the early morning hours, while NIR_V is at its minimum (Fig. S11) due to directional effects under direct illumination.

The overall nonlinear GPP–SIF_{tot} relationship (Fig. 3a) was mirrored by a similar NPQ–SIF_{tot} relationship (Fig. 4a), with NPQ measured at the leaf level. Even though the correlation between NPQ–SIF_{tot} was not significant when the pre-HW and HW periods were considered separately, the overall nonlinearity departed from the expected negative relationship reported in previous publications that did not account for heat stress (Magney *et al.*, 2017). Nonphotochemical quenching-GPP was instead markedly linear (Fig. 4b), and its slope was not altered by the HW (slope pre-HW = −1.2, slope HW = −0.98, $P = 0.77$),

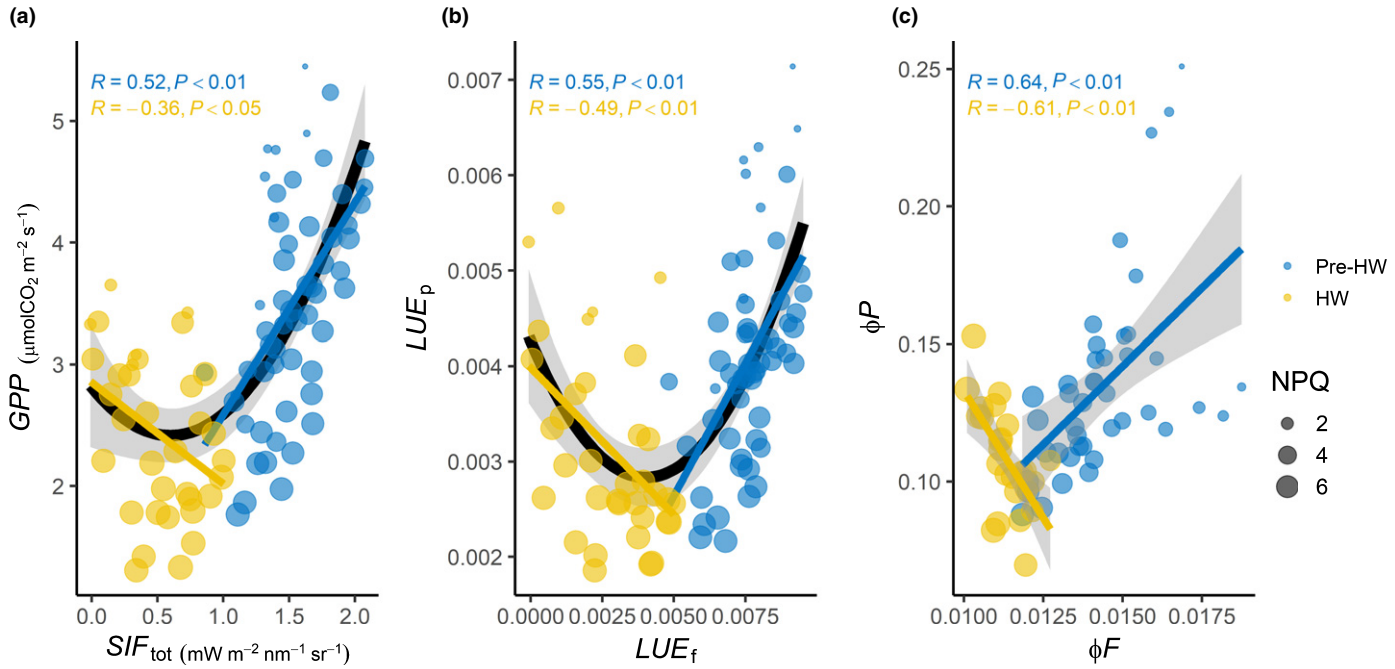

Fig. 3 (a) Scatterplot between gross primary production (GPP) and fluorescence emission at 760 nm total sun-induced fluorescence in the far-red region (SIF_{tot}). (b) Scatterplot between light-use efficiency of photosynthesis (LUE_p) and light-use efficiency of SIF emission ($LUEf_f$). In (b) the units of absorbed photosynthetic active radiation (APAR) for the LUE_p calculation are μmol m^{-2} s^{-1}, and the units of APAR for the LUE_f calculation are mW m^{-2} nm^{-1} sr^{-1}. (c) Scatterplot between yield of photochemistry (ΦP) and yield of fluorescence (ΦF). Blue points correspond to the pre-heatwave (pre-HW) period and yellow points correspond to the heatwave (HW) period. Hourly mean values in (a, b) are computed from 9 to 16 Coordinated Universal Time (UTC) and from 11 to 16 UTC in (c). The size of each point is proportional to the nonphotochemical quenching (NPQ). In each panel the Spearman's rank correlation coefficient (*R*) and *P*-value are reported for the pre-HW and HW period. The black line is the overall fit from a second-degree polynomial. Blue and yellow lines are linear regressions for the pre-HW and HW periods, respectively. The shaded area represents the 95% confidence interval of the fit.

suggesting that the photosynthetic activity of evergreen oaks was strongly controlled by the activity of the xanthophyll cycle. Nonphotochemical quenching was correlated with VPD ($R = 0.82$, $P < 0.01$), but the slope of NPQ–VPD showed a decreasing trend during the HW period (Fig. 4c) (slope pre-HW = 0.064, slope HW = 0.039, $P = 0.053$). In fact, the diurnal cycles of NPQ showed marked differences before and after the HW, with NPQ reaching a plateau in the afternoon of the HW period (Fig. 5a). In the same period, LUE_f exhibited a strong increase, highlighting changes in energy allocation during the HW. Additionally, the ΦP_{max} and the LUE_p values during the HW were strongly downregulated (Figs 5b, S3a,b), alongside the accumulation NPQ_s (Fig. S3c,d).

Nonphotochemical quenching, ϕP and ϕF plotted against *x* showed strong differences between the HW and pre-HW period (Fig. 6a,c,e). For *x* values higher than 0.75, NPQ-*x* was significantly positive in the pre-HW period ($R = 0.61$, $P < 0.01$), but showed a negative relationship during the HW ($R = -0.32$, $P < 0.01$) (Fig. 6b). The ΦNPQ shows a similar saturation, although less extreme than NPQ for high levels of *x* (Fig. S12a,b). ϕP-*x* presented a consistent negative relationship, but its slope became steeper during the HW (slope of −5.9 and −6.5, for pre-HW and HW respectively, $P < 0.01$) (Fig. 6d), meaning that, for the same *x*, ϕP decreases more during the HW. ϕF−*x* was negative during the pre-HW ($R = -0.47$, $P < 0.01$), but positive during the HW ($R = 0.57$, $P < 0.01$) (Fig. 6e). Taken together, this means that during the HW at high levels of light saturation, NPQ decreased, ϕP decreased faster than usual and ϕF increased.

Discussion

Previous research has highlighted the need to better understand the relationships between photosynthesis, fluorescence and NPQ under extreme stress conditions, to better exploit proximal and/or RS estimates of SIF for carbon cycle research (van der Tol *et al.*, 2014; Wohlfahrt *et al.*, 2018). Our study examined the effect of the HW on the GPP–SIF relationship in evergreen broadleaved trees, under no major changes in canopy structure. Our results showed that the HW caused nonlinearity in the overall relationship (i.e. when considering both the pre-HW and HW period together) between photochemistry and fluorescence at both canopy and leaf scale. We observed a saturation of NPQ at high temperatures, and a change in energy allocation towards fluorescence emission, therefore leading to the GPP–SIF nonlinear relationship when considering both the pre-HW and HW period. Additionally, current state-of-the-art radiative transfer and photosynthesis models such as SCOPE cannot model NPQ at the level of stress experienced in this study, suggesting that improved parametrisations are required to correctly model NPQ and SIF during extreme events.

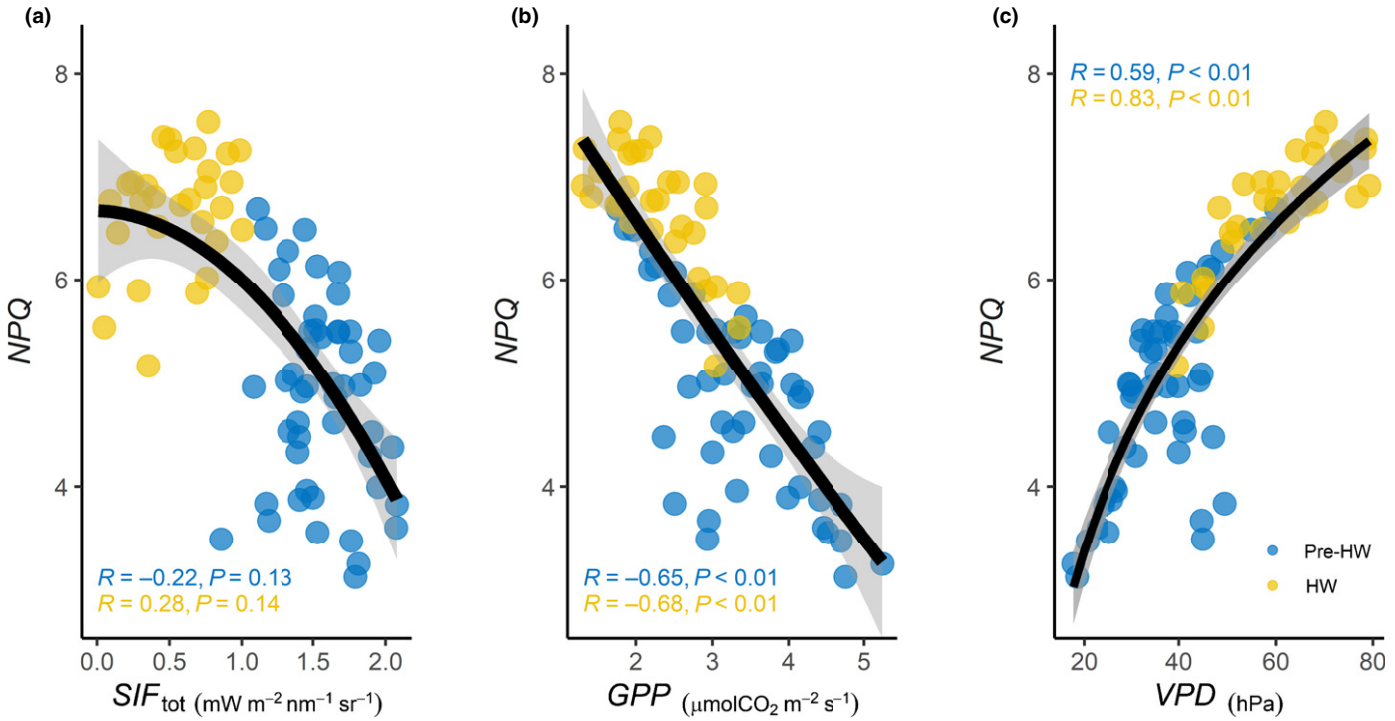

Fig. 4 (a) Scatterplot between nonphotochemical quenching (NPQ) and fluorescence emission at 760 nm, total sun-induced fluorescence in the far-red region (SIF_{tot}). (b) Scatterplot between NPQ and gross primary production (GPP). (c) Scatterplot between NPQ and vapour pressure deficit (VPD). Blue points correspond to the pre-heatwave (Pre-HW) period and yellow points correspond to the heatwave (HW) period. Hourly mean values are computed from 10 to 16 Coordinated Universal Time (UTC). In each panel the Spearman's rank correlation coefficient (R) and *P*-value are reported for the pre-HW and HW period. The black line is the overall fit from a second-degree polynomial. The shaded area represents the 95% confidence interval of the fit.

Unravelling the mechanism behind GPP–SIF nonlinearity in response to heat stress: the role of NPQ

We show that in Mediterranean evergreen broadleaved trees SIF responded to the extreme heat stress (Fig. 1d), indicating that SIF reflects changes in photosynthesis even in the absence of large changes in APAR and chlorophyll content. There is a current debate on the information content of SIF and the GPP–SIF relationship with two different positions (Dechant *et al.*, 2020): the first is that SIF contains both information about canopy structure but also physiological modulation of photosynthesis, the second is that SIF and GPP–SIF is mainly determined by structural changes. In this study we show that even with minimal changes in canopy structure (APAR and chlorophyll content) we observed a relationship between SIF–GPP, therefore challenging the studies suggesting that SIF–GPP is mainly determined by structure (Yang *et al.*, 2018). For comparison we showed that NDVI and NIR_V, two vegetation indices that contain information about vegetation structure, are limited at this time scale in which both directional effects and diffuse radiation do not allow tracking photosynthesis (Fig. S9b,c). It is worth noting that we cannot completely rule out subtle changes in canopy architecture, which might be caused by slight changes in leaf angle distribution (Gratani & Bombelli, 2000; Migliavacca *et al.*, 2017) or chloroplast movements (Van Wittenberghe *et al.*, 2019) in response to the high temperatures. However, the variations in Fesc (Fig. 2d) and other structural parameters seem extremely modest (Fig. 1e, f). Additionally, more diffuse radiation during the HW could have increased LUE_p or affected the reflectance. Still, reflectance-based vegetation indices would be only marginally affected by higher diffuse radiation according to simulations with the SCOPE model (Fig. S6). Moreover, the retrieval of SIF is more uncertain during the HW because of the lower SNR, which might explain the higher correlation of the ΦF–ΦP (leaf scale) compared with LUE_f–LUE_p (canopy scale) during the HW (Fig. 3b,c).

This study confirms that GPP–SIF is influenced by NPQ, the dominant dissipation pathway during the progression of the HW. Nonphotochemical quenching, which is observed with active fluorescence, can also be sensed at the top of canopy with PRI (Fig. S10d); the tight relationship between GPP and PRI (Fig. S9a) suggests the need for combining SIF and PRI for accurate GPP predictions under extreme heatwaves.

Leaf- and canopy-level observations agree markedly well (Fig. 3), indicating that some features of the leaf-level photosynthesis–fluorescence relationship manifest at the canopy level under the extreme heat stress experienced. This result calls for a more widespread combination of active and passive fluorescence measurements for explaining the partitioning of energy between NPQ, ϕP and ϕF, and how this is reflected in the GPP–SIF relationship. To do that, more analysis would be required to understand how the assumptions used when estimating PAM parameters (such as connectivity between PSII units) are affected at seasonal scale or by stress (Porcar-Castell, 2011).

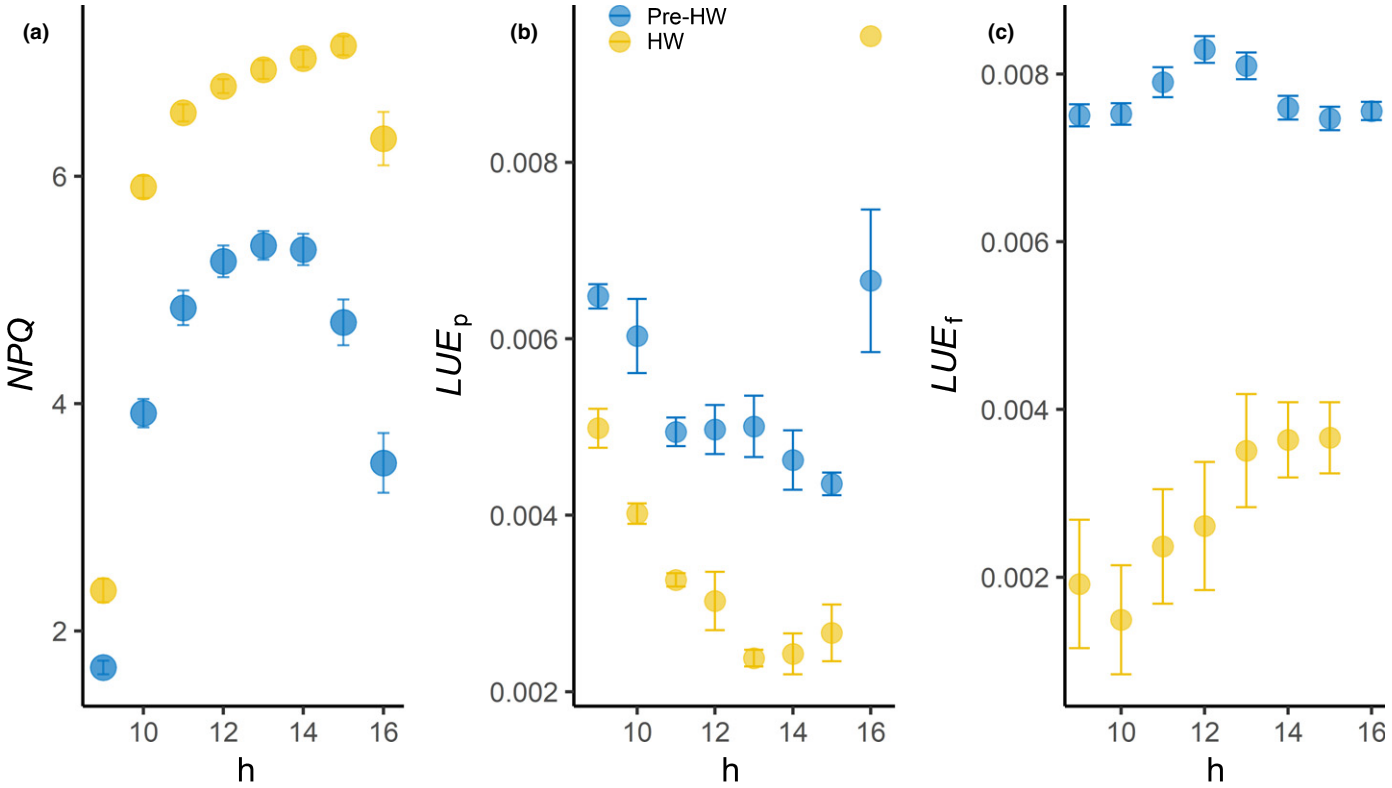

Fig. 5 Mean daily cycles for (a) nonphotochemical quenching (NPQ), (b) light-use efficiency of photosynthesis (LUE_p) and (c) light-use efficiency of sun-induced fluorescence in the far-red region (SIF) emission (LUE_f). Blue points correspond to the pre-heatwave (pre-HW) period and yellow points correspond to the heatwave (HW) period. Error bars correspond to the SE.

Nonphotochemical quenching exhibited a complex behaviour during the HW. Nonphotochemical quenching showed a strong response to VPD (Fig. 4c), indicating that stomatal closure may have been a process that triggered an increased dissipation of the excess energy through the NPQ mechanism. However, under high VPD (e.g. in the afternoon of the hotter days) the response of NPQ saturated, indicating that the temporal kinetics of stomata and the light reactions can decouple during heatwave events (Meinzer *et al.*, 2017). The apparent link between NPQ and stomatal conductance, also suggested in previous research (Medrano *et al.*, 2002; van der Tol *et al.*, 2009) and exploited through RS with the PRI index (Suárez *et al.*, 2008; Yang *et al.*, 2020), needs to be further investigated. In particular, a process-based understanding of the relationship between stomatal conductance, NPQ and SIF needs to be established to correctly use SIF as a proxy for transpiration. Under typical high illumination conditions ϕP and ϕF are positively correlated (Porcar-Castell *et al.*, 2014). This 'NPQ phase' is generally observed in most studies that linearly relate GPP and SIF (Damm *et al.*, 2010; Yang *et al.*, 2015) and is also representative of the pre-HW period. During the HW, plants do not have the capacity to adjust to unfamiliar extreme high temperatures and NPQ saturates, pushing the plant to the 'NPQ-saturation phase' (van der Tol *et al.*, 2014; Magney *et al.*, 2020). In this phase, NPQ saturates early in the day (Fig. 5a), leaving the photosystems without sufficient protection to cope with excess energy.

We propose that the mechanisms responsible for the observed GPP–SIF overall nonlinearity under high heat stress are shifts in energy allocation towards fluorescence emission (Fig. 5c), as the tree leaves are pushed by the extreme heat stress into the NPQ-saturation phase. The change in energy allocation would be caused by NPQ saturation and sustained photoinhibition. Nonphotochemical quenching might saturate if limited by its xanthophyll pool size, which has a turnover time of several days (Demmig *et al.*, 1988). Sustained photoinhibition is clearly demonstrated by a decrease in ΦP_{max} and an increase in NPQ_s (Fig. S3) and may be partly caused by damage to the reaction centres (Porcar-Castell *et al.*, 2008).

State-of-the-art radiative transfer and photosynthesis models cannot reproduce NPQ at high levels of stress

The fluorescence parameterisation in the state-of-the-art radiative transfer and photosynthesis models, such as SCOPE, is based on the relationship between the relative light saturation of photosynthesis and NPQ (Fig. 6a). van der Tol *et al.* (2014) reported this relationship for a variety of conditions, but not for the heat stress described in our study. Magney *et al.* (2020) indicated that there is only sparse evidence that under high stress conditions (high NPQ), an increase in ΦF can occur; therefore, more studies are needed to better interpret the GPP–SIF relationship. With our study we fill this gap and we show that the current parameterisation of models such as SCOPE that are used to derive photosynthesis and vegetation parameters from SIF measurements for current and future satellite missions, do not represent the NPQ response at the level of stress observed in our study (Fig. 6a,b). In fact, neither the NPQ levels

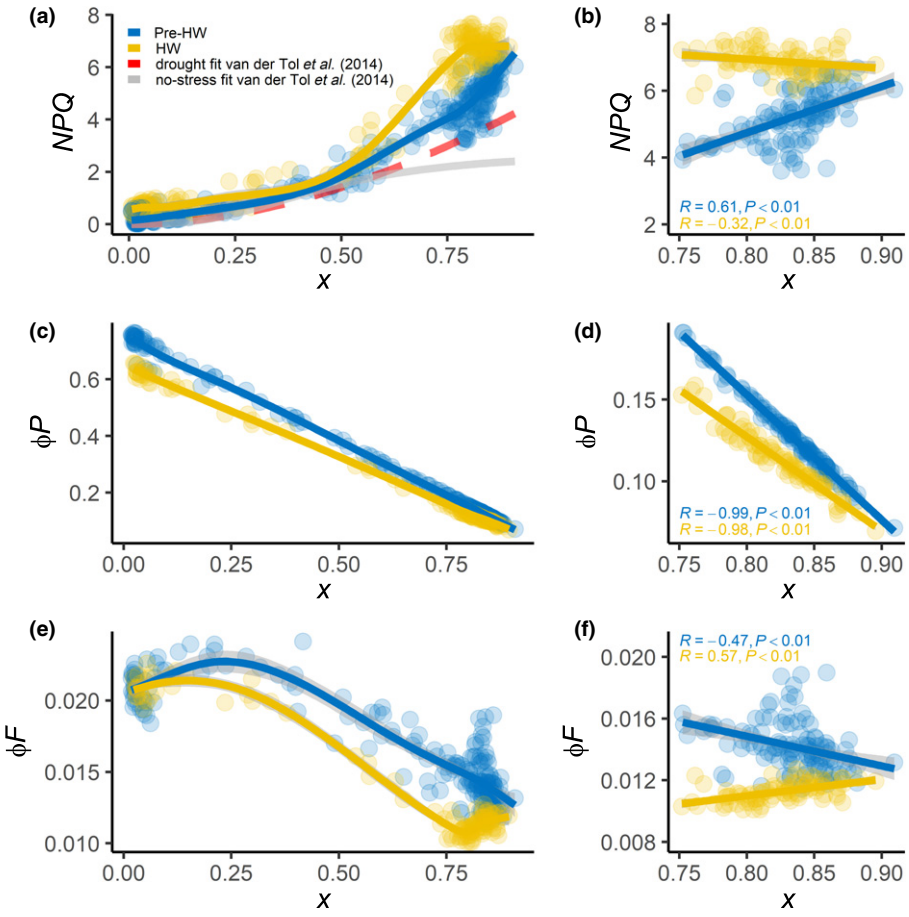

Fig. 6 (a, b) Scatterplot between nonphotochemical quenching (NPQ) and relative light saturation of photosynthesis (x). The red dashed line and solid grey line represent the NPQ–x fit for the drought stressed plants and nonstressed plants, respectively, from van der Tol *et al*. (2014). (c, d) Scatterplot between yield of photochemistry (ΦP) and x. (e, f) Scatterplot between yield of fluorescence (ΦF) and x. Blue points correspond to the pre-heatwave (pre-HW) period and yellow points correspond to the heatwave (HW) period. Hourly mean values with $x > 0.75$ are shown in (b, d, f). In (a, c, e) the lines are a local polynomial regression. In (b, d, f) the lines representing the linear regression and the Spearman's rank correlation coefficient (R) and P-value are reported for the pre-HW and HW period. The shaded area represents the 95% confidence interval of the fit.

reached in this study nor the observed nonlinearity of the NPQ-x relationship are reproduced by the model (Fig. 6a). Therefore, the model would not be able to describe the NPQ-saturation phase that led to the overall nonlinear response between SIF–GPP. This lack of description of the NPQ-saturation phase under extreme heat stress by SCOPE has to do with the fact that there is shortage of data constraining the process (van der Tol *et al*., 2014; Magney *et al*., 2020). The increasing availability of continuous passive and active fluorescence data, alongside NPQ estimates in multiple experimental sites., will provide the data to constrain the model parameterisation under different conditions, including during extreme events. Our results call for an improvement in the parameterisation of the relationship between the relative light saturation of photosynthesis and the NPQ process in radiative transfer and photosynthesis models. By doing so, we will probably improve the representation of GPP–SIF under extreme conditions with important implications for the exploitation of ground-based and satellite measurements to monitor photosynthetic performance of the vegetation.

Uncertainties related to footprint mismatch and leaf-canopy scaling

The difference between the radiometric and the EC footprint is a common source of uncertainty when analysing time series of spectral data and EC flux data. To minimise this uncertainty, the experiment was designed so that the FloX system and the MONI-PAM are installed within the EC footprint climatology (Fig. S1e), and the selected trees are representative of the trees in the footprint. Moreover, as the herbaceous vegetation in summer was completely senesced, the GPP signal is dominated by the photosynthesis of the *Quercus ilex* trees sampled (Perez-Priego *et al*., 2018; El-Madany *et al*., 2020). Another source of uncertainty is the mismatch between leaf-scale and canopy-scale measurements. To minimise the scale mismatch we sampled with the MONI-PAM and the FloX similar portions of the canopy of the two trees; that is the southern part of the canopy and external part of the crown. The sunlit leaves at the south side of the tree crown were sampled with the MONI-PAM because representatives of the portion of the crown that is in the field of view of the FloX. In this analysis we showed 15 d with stable structure of the canopy (no substantial changes in NDVI and SPAD). The stability of vegetation structure guarantees that, in the rather short period analysed, no artefacts affected the leaf to canopy scaling due to changes in leaf area or pigments. The good relationship we found between NPQ measured at leaf level and the PRI (Fig. S10d) is, for instance, an indicator of good comparability between leaf-level and canopy-scale measurements.

Conclusions

In sum, the present study shows that, under severe heatwaves, strong GPP–SIF nonlinearities are possible even in the absence of large changes in canopy structure. While a linear GPP–SIF relationship is expected in most conditions and driven by NPQ changes at the seasonal scale, under extreme stress a shift in energy allocation can occur. Our results can help to improve the parameterisation of the response of fluorescence to extreme events and in this way pave the way toward a more robust use of SIF for monitoring GPP under projected future climatic conditions characterised by increases in both the frequency and severity of heatwaves.

Acknowledgements

This project received funding from the European Union's Horizon 2020 research and innovation programme under the Marie Skłodowska-Curie grant agreement nos. 721995 and 749323. The authors acknowledge the Alexander von Humboldt Foundation for supporting this research with the Max-Planck Prize to Markus Reichstein. We also acknowledge the European Space Agency (ESA) in the frame of the FLEXSense campaign (ESA contract no. 4000125402/18/NL/NA) and the Photoproxy campaign (ESA contract no. 4000125731/19/NL/LF). MMigliavacca and GWohlfahrt acknowledge funding from the joint FWF-DFG DACH project 'Constraining terrestrial gross primary productivity by joint measurements of the carbonyl sulfide exchange and sun-induced fluorescence'. GWohlfahrt further acknowledges financial support by the AustroSIF project, which is funded by the FFG and BMK within the Austrian Space Applications Programme. Open access funding enabled and organised by ProjektDEAL.

Author contributions

DM and MM designed the study and carried out the majority of the data analysis. KS provided and processed the MONI-PAM data and contributed to the discussion. GW contributed to the discussion and helped to structure the manuscript. JP-L performed SCOPE runs and contributed to the discussion. JP-L and DM contributed to data sampling. CvdT, AP-C and TSM contributed to the discussion of the active fluorescence data. AC, RC, TE-M, RG-C, MPM, TJ, GM, UR, MReichstein, MRossini and MM contributed to the discussion and provided crucial feedback. All authors contributed to the discussion of the results and to the writing of the manuscript.

ORCID

Arnaud Carrara https://orcid.org/0000-0002-9095-8807
Roberto Colombo https://orcid.org/0000-0003-3997-0576
Tarek S. El-Madany https://orcid.org/0000-0002-0726-7141
Rosario Gonzalez-Cascon https://orcid.org/0000-0003-3468-0967
Troy S. Magney https://orcid.org/0000-0002-9033-0024
María Pilar Martín https://orcid.org/0000-0002-5563-8461
David Martini https://orcid.org/0000-0003-2180-5126
Mirco Migliavacca https://orcid.org/0000-0003-3546-8407
Gerardo Moreno https://orcid.org/0000-0001-8053-2696
Javier Pacheco-Labrador https://orcid.org/0000-0003-3401-7081
Albert Porcar-Castell https://orcid.org/0000-0003-1357-9982
Uwe Rascher https://orcid.org/0000-0002-9993-4588
Markus Reichstein https://orcid.org/0000-0001-5736-1112
Micol Rossini https://orcid.org/0000-0002-6052-3140
Karolina Sakowska https://orcid.org/0000-0003-4186-2558
Christiaan van der Tol https://orcid.org/0000-0002-2484-8191
Georg Wohlfahrt https://orcid.org/0000-0003-3080-6702

Data availability

Raw data and code are available and provided in an open access Zenodo repository through the 10.5281/zenodo.5773208.

References

Ač A, Malenovský Z, Olejníčková J, Gallé A, Rascher U, Mohammed G. 2015. Meta-analysis assessing potential of steady-state chlorophyll fluorescence for remote sensing detection of plant water, temperature and nitrogen stress. *Remote Sensing of Environment* **168**: 420–436.

Atherton J, Liu W, Porcar-Castell A. 2019. Nocturnal light emitting diode induced fluorescence (LEDIF): a new technique to measure the chlorophyll a fluorescence emission spectral distribution of plant canopies *in situ*. *Remote Sensing of Environment* **231**: 111137.

Badgley G, Field CB, Berry JA. 2017. Canopy near-infrared reflectance and terrestrial photosynthesis. *Science Advances* **3**: e1602244.

Barriopedro D, Sousa PM, Trigo RM, Garcia-Herrera R, Ramos AM. 2020. The exceptional Iberian heatwave of summer 2018. *Bulletin of the American Meteorological Society* **101**: S29–S33.

Bastos A, Ciais P, Friedlingstein P, Sitch S, Pongratz J, Fan L, Wigneron JP, Weber U, Reichstein M, Fu Z *et al.* 2020. Direct and seasonal legacy effects of the 2018 heat wave and drought on European ecosystem productivity. *Science Advances* **6**: eaba2724.

Beer C, Reichstein M, Tomelleri E, Ciais P, Jung M, Carvalhais N, Rödenbeck C, Arain MA, Baldocchi D, Bonan GB *et al.* 2010. Terrestrial gross carbon dioxide uptake: global distribution and covariation with climate. *Science* **329**: 834–838.

Beven K. 1979. A sensitivity analysis of the Penman-Monteith actual evapotranspiration estimates. *Journal of Hydrology* **44**: 169–190.

Bindoff NL, Stott PA, AchutaRao KM, Allen MR, Gillett N, Gutzler D, Hansingo K, Hegerl G, Hu YY, Jain S *et al.* 2014. *IPCC; Climate change 2013: The physical science basis.* Geneva, Switzerland: IPCC Working Group I Contribution to AR5, 867–952.

Cailly A. 1996. Fate of excitation at PS II in leaves. The non-photochemical side. *Plant Physiology and Biochemistry* **86**.

Cendrero-Mateo MP, Wieneke S, Damm A, Alonso L, Pinto F, Moreno J, Guanter L, Celesti M, Rossini M, Sabater N *et al.* 2019. Sun-induced chlorophyll fluorescence III: benchmarking retrieval methods and sensor characteristics for proximal sensing. *Remote Sensing* **11**: 962.

Damm A, Elbers J, Erler A, Gioli B, Hamdi K, Hutjes R, Kosvancova M, Meroni M, Miglietta F, Moersch A *et al.* 2010. Remote sensing of sun-induced fluorescence to improve modeling of diurnal courses of gross primary production (GPP). *Global Change Biology* **16**: 171–186.

Dechant B, Ryu Y, Badgley G, Zeng Y, Berry JA, Zhang Y, Goulas Y, Li Z, Zhang Q, Kang M *et al.* 2020. Canopy structure explains the relationship between photosynthesis and sun-induced chlorophyll fluorescence in crops. *Remote Sensing of Environment* **241**: 111733.

Demmig B, Winter K, Kruger A, Czygan FC. 1988. Zeaxanthin and the heat dissipation of excess light energy in nerium-oleander exposed to a combination of high light and water-stress. *Plant Physiology* **87**: 17–24.

Drake JE, Tjoelker MG, Vårhammar A, Medlyn B, Reich PB, Leigh A, Pfautsch S, Blackman CJ, López R, Aspinwall MJ *et al.* 2018. Trees tolerate an extreme heatwave via sustained transpirational cooling and increased leaf thermal tolerance. *Global Change Biology* **24**: 2390–2402.

El-Madany TS, Carrara A, Martin MP, Moreno G, Kolle O, Pacheco-Labrador J, Weber U, Wutzler T, Reichstein M, Migliavacca M. 2020. Drought and heatwave impacts on semi-arid ecosystems' carbon fluxes along a precipitation gradient. *Philosophical Transactions of the Royal Society B: Biological Sciences* **375**: 20190519.

El-Madany TS, Reichstein M, Perez-Priego O, Carrara A, Moreno G, Pilar Martín M, Pacheco-Labrador J, Wohlfahrt G, Nieto H, Weber U *et al.* 2018. Drivers of spatio-temporal variability of carbon dioxide and energy fluxes in a Mediterranean savanna ecosystem. *Agricultural and Forest Meteorology* **262**: 258–278.

Falge E, Baldocchi D, Olson R, Anthoni P, Aubinet M, Bernhofer C, Burba G, Ceulemans R, Clement R, Dolman H *et al.* 2001. Gap filling strategies for defensible annual sums of net ecosystem exchange. *Agricultural and Forest Meteorology* **107**: 43–69.

Fratini G, Mauder M. 2014. Towards a consistent eddy-covariance processing: an intercomparison of EddyPro and TK3. *Atmospheric Measurement Techniques* **7**: 2273–2281.

Gamon JA, Serrano L, Surfus JS. 1997. The photochemical reflectance index: an optical indicator of photosynthetic radiation use efficiency across species, functional types, and nutrient levels. *Oecologia* **112**: 492–501.

Garcia-Plazaola JI, Esteban R, Hormaetxe K, Fernandez-Marin B, Becerril JM. 2008. Photoprotective responses of Mediterranean and Atlantic trees to the extreme heat-wave of summer 2003 in Southwestern Europe. *Trees-Structure and Function* **22**: 385–392.

Genty B, Briantais J-M, Baker NR. 1989. The relationship between the quantum yield of photosynthetic electron transport and quenching of chlorophyll fluorescence. *Biochimica Et Biophysica Acta (BBA) – General Subjects* **990**: 87–92.

Georgieva K, Yordanov I. 1994. Temperature dependence of photochemical and non-photochemical fluorescence quenching in intact pea leaves. *Journal of Plant Physiology* **144**: 754–759.

Girden ER. 1992. *ANOVA: repeated measures*. Newbury Park, CA, USA: Sage.

Gonzalez-Cascon R, Jiménez-Fenoy L, Verdú-Fillola I, Martín MP. 2017. Aqueous-acetone extraction improves the drawbacks of using dimethylsulfoxide as solvent for photometric pigment quantification in *Quercus ilex* leaves. *Forest Systems* **26**: eSC04–eSC04.

Gratani L, Bombelli A. 2000. Correlation between leaf age and other leaf traits in three Mediterranean maquis shrub species: *Quercus ilex, Phillyrea latifolia* and *Cistus incanus*. *Environmental and Experimental Botany* **43**: 141–153.

Holmberg M, Aalto T, Akujärvi A, Arslan AN, Bergström I, Böttcher K, Lahtinen I, Mäkelä A, Markkanen T, Minunno F *et al.* 2019. Ecosystem services related to carbon cycling — modeling present and future impacts in boreal forests. *Frontiers in Plant Science* **10**: 343.

Julitta T, Burkart A, Colombo R, Rossini M, Schickling A, Migliavacca M, Cogliati S, Wutzler T, Rascher U. 2017. Accurate measurements of fluorescence in the O2A and O2B band using the FloX spectroscopy system—results and prospects. Proceedings of the Potsdam GHG flux workshop: from photosystems to ecosystems, Potsdam, Germany: 24–26.

Julitta T, Corp L, Rossini M, Burkart A, Cogliati S, Davies N, Hom M, Mac Arthur A, Middleton E, Rascher U *et al.* 2016. Comparison of sun-induced chlorophyll fluorescence estimates obtained from four portable field spectroradiometers. *Remote Sensing* **8**: 122.

Kitajima M, Butler WL. 1975. Quenching of chlorophyll fluorescence and primary photochemistry in chloroplasts by dibromothymoquinone. *Biochimica et Biophysica Acta* **376**: 105–115.

Knauer J, El-Madany TS, Zaehle S, Migliavacca M. 2018. Bigleaf—An R package for the calculation of physical and physiological ecosystem properties from eddy covariance data. *PLoS ONE* **13**: e0201114.

Lasslop G, Reichstein M, Papale D, Richardson AD, Arneth A, Barr A, Stoy P, Wohlfahrt G. 2010. Separation of net ecosystem exchange into assimilation and respiration using a light response curve approach: critical issues and global evaluation. *Global Change Biology* **16**: 187–208.

Li Z, Moreau L. 1996. A new approach for remote sensing of canopy-absorbed photosynthetically active radiation. I: total surface absorption. *Remote Sensing of Environment* **55**: 175–191.

Luo Y, El-Madany TS, Filippa G, Ma X, Ahrens B, Carrara A, Gonzalez-Cascon R, Cremonese E, Galvagno M, Hammer TW *et al.* 2018. Using near-infrared-enabled digital repeat photography to track structural and physiological phenology in mediterranean tree–grass ecosystems. *Remote Sensing* **10**: 1293.

Luo Y, El-Madany T, Ma X, Nair R, Jung M, Weber U, Filippa G, Bucher SF, Moreno G, Cremonese E *et al.* 2020. Nutrients and water availability constrain the seasonality of vegetation activity in a Mediterranean ecosystem. *Global Change Biology* **26**: 4379–4400.

Magney TS, Barnes ML, Yang X. 2020. On the covariation of chlorophyll fluorescence and photosynthesis across scales. *Geophysical Research Letters* **47**: e2020GL091098.

Magney TS, Bowling DR, Logan BA, Grossmann K, Stutz J, Blanken PD, Burns SP, Cheng R, Garcia MA, Kohler P *et al.* 2019. Mechanistic evidence for tracking the seasonality of photosynthesis with solar-induced fluorescence. *Proceedings of the National Academy of Sciences, USA* **116**: 11640–11645.

Magney TS, Frankenberg C, Fisher JB, Sun Y, North GB, Davis TS, Kornfeld A, Siebke K. 2017. Connecting active to passive fluorescence with photosynthesis: a method for evaluating remote sensing measurements of Chl fluorescence. *New Phytologist* **215**: 1594–1608.

Mauder M, Foken T. 2011. *Documentation and instruction manual of the eddy-covariance software package TK3*. [WWW document] URL https://epub.uni-bayreuth.de/342/1/ARBERG046.pdf [accessed 12 June 2021].

Medrano H, Escalona JM, Bota J, Gulías J, Flexas J. 2002. Regulation of photosynthesis of C3 plants in response to progressive drought: stomatal conductance as a reference parameter. *Annals of Botany* **89**: 895–905.

Meinzer FC, Smith DD, Woodruff DR, Marias DE, McCulloh KA, Howard AR, Magedman AL. 2017. Stomatal kinetics and photosynthetic gas exchange along a continuum of isohydric to anisohydric regulation of plant water status. *Plant Cell and Environment* **40**: 1618–1628.

Meroni M, Rossini M, Guanter L, Alonso L, Rascher U, Colombo R, Moreno J. 2009. Remote sensing of solar-induced chlorophyll fluorescence: review of methods and applications. *Remote Sensing of Environment* **113**: 2037–2051.

Migliavacca M, Perez-Priego O, Rossini M, El-Madany TS, Moreno G, van der Tol C, Rascher U, Berninger A, Bessenbacher V, Burkart A *et al.* 2017. Plant functional traits and canopy structure control the relationship between photosynthetic CO_2 uptake and far-red sun-induced fluorescence in a Mediterranean grassland under different nutrient availability. *New Phytologist* **214**: 1078–1091.

Moreau L, Li Z. 1996. A new approach for remote sensing of canopy absorbed photosynthetically active radiation. II: proportion of canopy absorption. *Remote Sensing of Environment* **55**: 192–204.

Moreno J, Goulas Y, Huth A, Middleton E, Miglietta F, Mohammed G, Nedbal L, Rascher U, Verhoef W, Drusch M. 2015. *Report for mission selection: fLEX. FLEX (ESA SP-1330/2, June 2015)*. Noordwijk, the Netherlands: ESA Communications.

Ogaya R, Peñuelas J. 2003. Comparative seasonal gas exchange and chlorophyll fluorescence of two dominant woody species in a Holm Oak forest. *Flora-Morphology, Distribution, Functional Ecology of Plants* **198**: 132–141.

Pacheco-Labrador J, Hueni A, Mihai L, Sakowska K, Julitta T, Kuusk J, Sporea D, Alonso L, Burkart A, Cendrero-Mateo MP *et al.* 2019a. Sun-induced chlorophyll fluorescence I: instrumental considerations for proximal spectroradiometers. *Remote Sensing* **11**: 960.

Pacheco-Labrador J, Perez-Priego O, El-Madany TS, Julitta T, Rossini M, Guan J, Moreno G, Carvalhais N, Martín MP, Gonzalez-Cascon R *et al.* 2019b. Multiple-constraint inversion of SCOPE. Evaluating the potential of GPP and SIF for the retrieval of plant functional traits. *Remote Sensing of Environment* **234**: 111362.

Papale D, Reichstein M, Aubinet M, Canfora E, Bernhofer C, Kutsch W, Longdoz B, Rambal S, Valentini R, Vesala T *et al.* 2006. Towards a standardized processing of net ecosystem exchange measured with eddy covariance technique: algorithms and uncertainty estimation. *Biogeosciences* **3**: 571–583.

Perez-Priego O, El-Madany TS, Migliavacca M, Kowalski AS, Jung M, Carrara A, Kolle O, Martín MP, Pacheco-Labrador J, Moreno G *et al.* 2017. Evaluation of eddy covariance latent heat fluxes with independent lysimeter and sapflow estimates in a Mediterranean savannah ecosystem. *Agricultural and Forest Meteorology* **236**: 87–99.

Perez-Priego O, Katul G, Reichstein M, El-Madany TS, Ahrens B, Carrara A, Scanlon TM, Migliavacca M. 2018. Partitioning eddy covariance water flux components using physiological and micrometeorological approaches. *Journal of Geophysical Research: Biogeosciences* **123**: 3353–3370.

Porcar-Castell A. 2011. A high-resolution portrait of the annual dynamics of photochemical and non-photochemical quenching in needles of *Pinus sylvestris*. *Physiologia Plantarum* **143**: 139–153.

Porcar-Castell A, Juurola E, Ensminger I, Berninger F, Hari P, Nikinmaa E. 2008. Seasonal acclimation of photosystem II in *Pinus sylvestris*. II. Using the rate constants of sustained thermal energy dissipation and photochemistry to study the effect of the light environment. *Tree Physiology* **28**: 1483–1491.

Porcar-Castell A, Tyystjarvi E, Atherton J, van der Tol C, Flexas J, Pfundel EE, Moreno J, Frankenberg C, Berry JA. 2014. Linking chlorophyll a fluorescence to photosynthesis for remote sensing applications: mechanisms and challenges. *Journal of Experimental Botany* **65**: 4065–4095.

Reichstein M, Bahn M, Ciais P, Frank D, Mahecha MD, Seneviratne SI, Zscheischler J, Beer C, Buchmann N, Frank DC *et al.* 2013. Climate extremes and the carbon cycle. *Nature* **500**: 287–295.

Reichstein M, Falge E, Baldocchi D, Papale D, Aubinet M, Berbigier P, Bernhofer C, Buchmann N, Gilmanov T, Granier A *et al.* 2005. On the separation of net ecosystem exchange into assimilation and ecosystem respiration: review and improved algorithm. *Global Change Biology* **11**: 1424–1439.

Rutherford A. 2001. *Introducing ANOVA and ANCOVA: a GLM approach.* Thousand Oaks, CA, USA: Sage.

Sousa PM, Barriopedro D, Ramos AM, Garcia-Herrera R, Espirito-Santo F, Trigo RM. 2019. Saharan air intrusions as a relevant mechanism for Iberian heatwaves: the record breaking events of August 2018 and June 2019. *Weather and Climate Extremes* **26**: 100224.

Suárez L, Zarco-Tejada PJ, Sepulcre-Cantó G, Pérez-Priego O, Miller J, Jiménez-Muñoz J, Sobrino J. 2008. Assessing canopy PRI for water stress detection with diurnal airborne imagery. *Remote Sensing of Environment* **112**: 560–575.

Teskey R, Wertin T, Bauweraerts I, Ameye M, McGuire MA, Steppe K. 2015. Responses of tree species to heat waves and extreme heat events. *Plant, Cell & Environment* **38**: 1699–1712.

Thom A. 1972. Momentum, mass and heat exchange of vegetation. *Quarterly Journal of the Royal Meteorological Society* **98**: 124–134.

van der Tol C, Berry JA, Campbell PKE, Rascher U. 2014. Models of fluorescence and photosynthesis for interpreting measurements of solar-induced chlorophyll fluorescence. *Journal of Geophysical Research: Biogeosciences* **119**: 2312–2327.

van der Tol C, Verhoef W, Rosema A. 2009. A model for chlorophyll fluorescence and photosynthesis at leaf scale. *Agricultural and Forest Meteorology* **149**: 96–105.

Uddling J, Gelang-Alfredsson J, Piikki K, Pleijel H. 2007. Evaluating the relationship between leaf chlorophyll concentration and SPAD-502 chlorophyll meter readings. *Photosynthesis Research* **91**: 37–46.

Van Wittenberghe S, Alonso L, Malenovsky Z, Moreno J. 2019. *In vivo* photoprotection mechanisms observed from leaf spectral absorbance changes showing VIS-NIR slow-induced conformational pigment bed changes. *Photosynthesis Research* **142**: 283–305.

Wohlfahrt G, Gerdel K, Migliavacca M, Rotenberg E, Tatarinov F, Muller J, Hammerle A, Julitta T, Spielmann FM, Yakir D. 2018. Sun-induced fluorescence and gross primary productivity during a heat wave. *Scientific Reports* **8**: 1–9.

Wong CY, Gamon JA. 2015. Three causes of variation in the photochemical reflectance index (PRI) in evergreen conifers. *New Phytologist* **206**: 187–195.

Wutzler T, Lucas-Moffat A, Migliavacca M, Knauer J, Sickel K, Sigut L, Menzer O, Reichstein M. 2018. Basic and extensible post-processing of eddy covariance flux data with REddyProc. *Biogeosciences* **15**: 5015–5030.

Yang JC, Magney TS, Yan D, Knowles JF, Smith WK, Scott RL, Barron-Gafford GA. 2020. The photochemical reflectance index (PRI) captures the ecohydrologic sensitivity of a semiarid mixed conifer forest. *Journal of Geophysical Research: Biogeosciences* **125**: e2019JG005624.

Yang K, Ryu Y, Dechant B, Berry JA, Hwang Y, Jiang C, Kang M, Kim J, Kimm H, Kornfeld A *et al.* 2018. Sun-induced chlorophyll fluorescence is more strongly related to absorbed light than to photosynthesis at half-hourly resolution in a rice paddy. *Remote Sensing of Environment* **216**: 658–673.

Yang PQ, van der Tol C. 2018. Linking canopy scattering of far-red sun-induced chlorophyll fluorescence with reflectance. *Remote Sensing of Environment* **209**: 456–467.

Yang X, Tang J, Mustard JF, Lee JE, Rossini M, Joiner J, Munger JW, Kornfeld A, Richardson AD. 2015. Solar-induced chlorophyll fluorescence that correlates with canopy photosynthesis on diurnal and seasonal scales in a temperate deciduous forest. *Geophysical Research Letters* **42**: 2977–2987.

Zeng Y, Badgley G, Dechant B, Ryu Y, Chen M, Berry JA. 2019. A practical approach for estimating the escape ratio of near-infrared solar-induced chlorophyll fluorescence. *Remote Sensing of Environment* **232**: 111209.

Zhang Y, Guanter L, Berry JA, Joiner J, van der Tol C, Huete A, Gitelson A, Voigt M, Köhler P. 2014. Estimation of vegetation photosynthetic capacity from space-based measurements of chlorophyll fluorescence for terrestrial biosphere models. *Global Change Biology* **20**: 3727–3742.

Supporting Information

Additional Supporting Information may be found online in the Supporting Information section at the end of the article.

Fig. S1 Picture of the eddy covariance tower, the radiometric tower, the MONI-PAM system and satellite picture of the experimental site at Majadas de Tiétar.

Fig. S2 2D kernel density estimation of daily maximum T_{air} and daily maximum vapour pressure deficit (VPD) from 2004 to 2018 in the months of June, July and August.

Fig. S3 Scatterplot between ΦP_{max} and daily means of sun-induced fluorescence in the far-red region (SIF) and vapour pressure deficit (VPD). Scatterplot between daily means of the sustained component of nonphotochemical quenching (NPQ_s) and SIF and VPD.

Fig. S4 Mean daily cycles for light-use efficiency of photosynthesis (LUEp), light-use efficiency of fluorescence emission (LUE_f), x, ΦP, ΦF and nonphotochemical quenching.

Fig. S5 Scatterplot between gs and vapour pressure deficit (VPD).

Fig. S6 Simulations with the soil canopy observation, photochemistry and energy fluxes (SCOPE) model on the effect of diffuse to total radiation on normalised difference vegetation index (NDVI), near-infrared reflectance of vegetation index (NIR_V), photochemical reflectance index (PRI) and sun-induced fluorescence in the far-red region (SIF).

Fig. S7 Scatterplot between light-use efficiency of photosynthesis (LUEp) and light-use efficiency of fluorescence emission (LUE_f).

Scatterplot between nonphotochemical quenching (NPQ) and gross primary production (GPP).

Fig. S8 Relationship between ϕP and ϕF for the pre-heatwave (pre-HW) period and for the HW period.

Fig. S9 Scatterplot between gross primary production (GPP) and photochemical reflectance index (PRI). Scatterplot between GPP and normalised difference vegetation index (NDVI). Scatterplot between GPP and near-infrared reflectance of vegetation index (NIR_V).

Fig. S10 Scatterplot between ΦF and light-use efficiency of fluorescence emission (LUE_f). Scatterplot between ΦP and light-use efficiency of photosynthesis (LUEp). Scatterplot between ΦF $SIF_{660\text{-}840}$. Scatterplot between nonphotochemical quenching (NPQ) and the photochemical reflectance index (PRI).

Fig. S11 Hourly means of vapour pressure deficit (VPD), shortwave incoming radiation (SWin), normalised difference vegetation index (NDVI), near-infrared reflectance of vegetation index (NIR_V), light-use efficiency of photosynthesis (LUEp), light-use efficiency of fluorescence emission ($LUEf_f$), nonphotochemical quenching (NPQ), ΦP and ΦF.

Fig. S12 Scatterplot between ΦNPQ and *x*.

Table S1 Spearman's rank correlation coefficient (R) and *P*-value between compared variables (SIF).

Table S2 Spearman's rank correlation coefficient (R) and *P*-value between compared variables (GPP–SIF).

Table S3 Spearman's rank correlation coefficient (R) and *P*-value between compared variables (GPP–VDP).

Please note: Wiley Blackwell are not responsible for the content or functionality of any Supporting Information supplied by the authors. Any queries (other than missing material) should be directed to the *New Phytologist* Central Office.